Applied Surface Science 507 (2020) 145136

Contents lists available at ScienceDirect

Applied Surface Science

journal homepage: www.elsevier.com/locate/apsusc

Full Length Article

Nanosecond laser-based high-throughput surface nanostructuring (nHSN)

Qinghua Wang[a,1], Avik Samanta[a,1], Scott K. Shaw[b], Hui Hu[c], Hongtao Ding[a,*]

[a] Department of Mechanical Engineering, The University of Iowa, Iowa City, IA 52242, USA
[b] Department of Chemistry, The University of Iowa, Iowa City, IA 52242, USA
[c] Department of Aerospace Engineering, Iowa State University, 2271 Howe Hall, Room 1200, Ames, IA 50011, USA

ARTICLE INFO

Keywords:
Laser surface texturing
Chemical modification
Nanostructuring
Superhydrophobic
Superhydrophilic

ABSTRACT

We present a novel nanosecond laser-based high-throughput surface nanostructuring (nHSN) process that can simultaneously create random nanostructures and attain desirable surface chemistry over large-area metal alloy surfaces. nHSN consists of two sequential steps: (1) nanosecond laser texturing (NLT) and (2) chemical immersion treatment (CIT). NLT step in water confinement (wNLT) does not generate topological patterns but preconditions the metal surface chemically and mechanically. Our analysis shows that surface nanostructuring results from a combined effect of chemical etching and attachment of functional groups during the CIT phase of nHSN. A proper silane reagent can be selected for the CIT phase to achieve the desired surface wetting behavior, while laser parameters can also be adjusted during the NLT phase to finely tune the nanostructuring mechanism. nHSN nanostructures with fluorosilane chemistry repel water, while those with cyanosilane chemistry attract water. Extreme wettability including superhydrophobicity and superhydrophilicity is assessed for multiple engineering metal alloys including aluminum, steel and titanium alloys. Compared with existing ultrashort laser-based surface-texturing methods, the nHSN laser scan time represents a significant improvement in processing efficiency and enables a practical throughput for large-area processing of engineering alloys.

1. Introduction

In nature, many materials possess delicate surface nanostructures that render outstanding surface functionalities. In recent years, researchers have begun to artificially engineer metal alloy surfaces with different types of surface nanostructures [1,2]. These metal surface nanostructures can exhibit extreme wetting properties, i.e., superhydrophobicity or superhydrophilicity, which has led to many innovative applications, including anti-icing [3], drag reduction [4], self-cleaning [5] and anti-bacterial surface treatment [6]. A number of surface processing/fabrication techniques have been developed for metal alloys to produce nanostructures for extreme surface wettability applications. These techniques can be categorized into three main approaches: (a) the top-down approach, (b) the bottom-up approach and (c) the combined approach. The top-down approach removes material from a bulk workpiece and creates nanoscale structures using energy sources and chemical and electrochemical processes. Typical top-down approaches include etching [7], anodization [8] and lithography [9]. The bottom-up approach builds nanoscale features via nano-manufacturing of atomic and molecular-scale components. Typical bottom-up approaches include electrodeposition [10], electrospinning [11] and the sol-gel method [12]. A combined approach incorporates both top-down and bottom-up approaches [13] to fabricate surface structures. However, each of these approaches has some distinct drawbacks that limit their practicability and reliability. For example, lithography, electrodeposition and electrospinning require expensive equipment and are very time-consuming. Etching and anodization, on the other hand, are time- and cost-efficient, but their process flexibility and precision are very low. A combined approach might increase process precision, but it would require complex manufacturing procedures, and the production cost and time consumption would be extremely high. The above-mentioned disadvantages and limitations make it difficult to fabricate large surface areas effectively using these methods. There is an urgent need for the development of new technologies that can efficiently fabricate surface nanostructures.

Laser-based surface-texturing methods have emerged in the last decade as a popular top-down approach demonstrating the significant advantages of high precision and process flexibility. These existing technologies frequently utilize ultrashort pulse lasers, e.g., femtosecond lasers or picosecond lasers, to fabricate either a laser-induced periodic surface structure (LIPSS) [14,15] or laser-inscribed hierarchical or dual-scale surface structures [16,17] on metal surfaces. A LIPSS typically

* Corresponding author.
E-mail address: hongtao-ding@uiowa.edu (H. Ding).
[1] Contributed equally to this work.

https://doi.org/10.1016/j.apsusc.2019.145136
Received 9 September 2019; Received in revised form 13 December 2019; Accepted 19 December 2019
Available online 23 December 2019
0169-4332/

consists of laser-induced surface ripples with a periodicity equal to or smaller than the wavelength of the laser radiation (much smaller than the effective laser spot size). These LIPSS ripples are self-organized surface structures, and their periods vary based on the laser fluence applied. The hierarchical structure consists of ordered microstructures (e.g., parallel microgrooves/microtrenches/microspikes/spot array) and laser-induced random or periodic nanostructures on top of the microstructures. These ultrashort pulse lasers often scan line profiles with a very fine spatial resolution of a few tens of micrometers and require several pulses per spot to create the desired surface structures. The surface scanning efficiency is usually kept low because of the high spatial resolution needed. As a result, the processing speed and process throughput are very low for those processing techniques [18,19]. It takes several minutes to several hours to texture a 1 in^2 metal surface [20,21]. Consequently, the laser-texturing methods that use ultrashort pulse lasers are limited to processing small areas. This also restricts these laser-texturing techniques from being adopted for commercial usage to treat large surface areas for industrial applications. Hierarchical structures can also be created by single-step nanosecond laser irradiation [5,23–25]. Microscale surface features like microtrenches/microgrooves [5], micromatrix/crosshatch [25] or spot arrays [23,24] were generated by nanosecond laser pulsed irradiation. The random nanoscale features were dispersed on top of the microscale features due to the re-solidification of the ablated materials. Even though some latest research works on nanosecond laser texturing have increased the laser texturing rate up to 4.5 cm^2/min [26–28], the processing speed is still not high enough to enable large-area surface processing. The laser-texturing community has welcomed exploration of an alternate approach to improve processing efficiency and reduce production cost [18] while keeping the performance comparable with the existing methods.

Wettability of a micro/nanostructured surface results from a combined effect of surface topography and surface chemistry. Immediately after laser texturing, a metal surface usually behaves as if it was hydrophilic. Three main chemistry modification methods have been applied to make a laser-textured surface superhydrophobic: storage in air for 15–30 days [24,29], low-temperature heat treatment [30–32] and chemical coating [14,15]. Storage in air is a very uncontrolled, lengthy process, and the process mechanism includes organic adsorption from air onto the textured surface [29]. Therefore, the time to achieve superhydrophobicity often varies from location to location due to the variation in organic constituents in the atmosphere. The mechanism of achieving superhydrophobicity using low-temperature heat treatment is very similar to storage in air. It occurs due to the accelerated adsorption of organic constituents when kept in air after the heat treatment [30]. This process reduces the required time from several days to one day or a few hours. The most suitable solution to achieve superhydrophobicity is to perform a chemical treatment after laser texturing; this produces a durable superhydrophobic surface in a short period.

Although a superhydrophilic surface can also be fabricated by laser texturing, there has been limited research in this direction. Achieving a sustainable laser-textured superhydrophilic surface also requires surface chemistry modification after the laser-texturing process. Generally, two processes have been explored to achieve superhydrophilicity on laser-textured metals: boiling water treatment [31] and high-temperature heat treatment [29]. The boiling water treatment created a pseudoboehmite nanostructure in aluminum with enriched −OH groups to achieve superhydrophilicity [31]. However, this process does not apply to some metals and metal alloys like iron or steel, which see detrimental effects when kept in hot water. Superhydrophilicity was also achieved by a high-temperature heat treatment by burning out the absorbed organic constituents on the textured surface [29]. However, a high-temperature heat treatment might induce other effects like re-crystallization and grain orientation change, the effects of which on wettability are still unknown. On the other hand, research on the chemical treatment of laser-textured metal to make it superhydrophilic has not yet been conducted.

There are two major issues with the existing laser-based metal-surface-texturing methods: (1) the low process throughput, and (2) lack of appreciation of the roles of surface chemistry for laser-textured surfaces. Indeed, a significant knowledge gap exists in the current literature on the role of surface chemistry on laser-textured surface structures, and this has significantly limited the further development of these laser-based technologies. A systematic understanding of the interdependence of laser-textured surface structure and surface chemistry modification is required. Development of a new laser-based technique for fast, scalable surface nanostructuring is critically needed for extreme surface wettability applications.

In this work, a novel nanosecond laser-based high-throughput surface nanostructuring (nHSN) process was developed to simultaneously create random nanostructures and attain desirable surface chemistry over large-area metal alloy surfaces. A preparatory study was carried out on the nHSN process to investigate the feasibility of the process design [33–35] and secure the novelty of the process [36]. This study includes a complete analysis of the process for multiple materials in two extreme wettability scenarios: superhydrophobicity and superhydrophilicity. nHSN experiments were performed on multiple engineering alloys including AISI 4130 steel, aluminum alloy (AA 6061) and titanium alloy (Ti-6Al-4V) to produce these two extreme wetting conditions. The mechanism of nanostructure generation and surface chemistry change was investigated using a scanning electron microscope (SEM), X-ray photoelectron spectroscopy (XPS) and inductively coupled plasma-optical emission spectroscopy (ICP-OES) analyses.

2. nHSN process

2.1. Process development

To develop the nHSN process, a Q-switched Nd:YAG nanosecond laser (wavelength 1064 nm), which emits a pulse duration of 6–8 ns and a pulse energy on the order of hundreds of mJ, was used in the nanosecond laser texturing (NLT) step. A 3-axis galvanometer laser scanner (SCANLAB intelliSCAN® 20 and varioSCAN$_{de}$ 40i), configured with an f-theta objective, served to direct the laser scanning of the metal surface. Various laser-processing modes were initially investigated for process development, including nanosecond laser texturing in air (aNLT) and water-confined nanosecond laser texturing (wNLT). During wNLT, the metal workpiece is submerged in deionized (DI) water, thereby confining the laser-induced plasma and surface-enhancing effects. In contrast to conventional laser-texturing methods [5,20,25,37–41], wNLT is novel in its application of high energy radiation as nanosecond pulses at a coarse spatial resolution and under water confinement.

After the laser-texturing step, a chemical immersion treatment (CIT) was developed to induce surface chemistry modification of the laser-treated surfaces by immersion in a silane reagent solution. For the initial set of experiments, the laser-textured material was immersed in an ethanol solution of 1.5 wt% chlorosilane reagent [$CF_3(CF_2)_5(CH_2)_2SiCl_3$], also known as FOTS, at room temperature for ~3 h. Workpieces were then cleaned and dried using compressed nitrogen. The CIT process is easier to operate and more efficient than conventional surface-texturing methods [14,15] that achieve surface silane modification through deposition of evaporated silane reagents under vacuum conditions and elevated temperatures.

Water contact angle (θ_w) was used in this experimental analysis to characterize the surface wettability, which describes the tendency of a liquid to spread into or repel from a solid metal surface. The surface wettability of water can be categorized into four categories: hydrophobic, hydrophilic, superhydrophobic and superhydrophilic [42]. Using θ_w of 90° as a threshold, surfaces are divided into hydrophobic surface ($\theta_w > 90°$) and hydrophilic surface ($\theta_w < 90°$). θ_w with a value less than 10° is designated as superhydrophilic, and the water completely spreads over the surface. θ_w with a value between 10° and

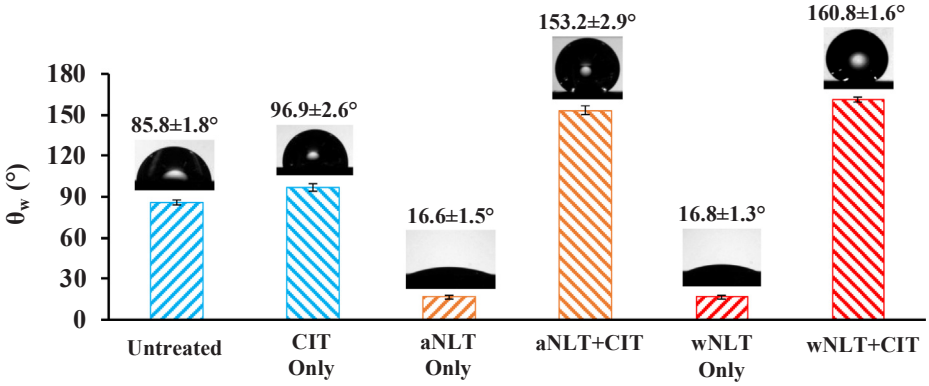

Fig. 1. Water contact angle θ_w measurement results for AISI 4130 steel specimens treated with various process conditions: nanosecond laser texturing in air (aNLT), water confined nanosecond laser texturing (wNLT), chemical immersion treatment (CIT), and combinations thereof.

90° is categorized as hydrophilic, while surfaces with θ_w between 90° and 150° are designated as hydrophobic. When θ_w is greater than 150°, the surface is generally regarded as superhydrophobic.

The θ_w measurement results are shown in Fig. 1 for AISI 4130 steel specimens, which were treated with various experimental combinations. Uncertainty in these θ_w measurements was typically on the level of a few degrees, and the averaged measurement value was used in the following discussions. θ_w was 85.8° for an AISI 4130 steel specimen without any treatment and increased to 96.9° after CIT treatment, indicating that the CIT process alone does not significantly alter surface wettability. aNLT produced a highly hydrophilic surface with a θ_w less than 20° shortly after (within several hours of) laser texturing. With CIT, the θ_w of the aNLT specimen surface increased to 153.2°. wNLT also produced a highly hydrophilic surface with a θ_w less than 20° shortly after laser texturing. However, with the CIT step directly following wNLT, the θ_w of the resultant surface dramatically increased to 161°. Both aNLT and wNLT, in conjunction with CIT, produced superhydrophobic surfaces with θ_w greater than 150°. wNLT rendered higher θ_w, mainly due to the use of water as a confinement medium, which confines the laser-induced plasma and enhances the surface-texturing effects. More importantly, wNLT significantly improves processing efficiency by employing nanosecond laser texturing under water confinement. For instance, a 5 mm-diameter laser spot (D) and a large laser line spacing of 2 mm were applied during wNLT, substantially reducing specific laser scanning time, t_s, from hundreds of minutes per square inch (using a femtosecond or picosecond laser [20,21,43]) and several minutes (using a nanosecond laser [26,41,44]) to ~10 s/in^2. This breakthrough yields a feasible treatment pathway for macroscale metal surfaces.

In summary, the optimized nHSN process comprises two sequential steps of NLT and CIT, as illustrated in Fig. 2. NLT can not only precondition a large-area metal surface using a rapid scanning mode, but also scan a complex surface profile following computer-generated paths. It can be performed under water (wNLT) or in air (aNLT) using a wide range of laser operating parameters. CIT is a simple procedure for creating nanostructures over the laser-textured areas and attaining the desired chemistry. In this study, fluorosilane and cyanosilane can be used to achieve superhydrophobicity and superhydrophilicity, respectively. Fluorosilane reagents are selected for the CIT process to achieve superhydrophobicity due to the presence of -CF_2- and -CF_3 groups in their chemical structure, which are known to reduce the surface energy [41,45]. Besides the aforementioned FOTS, 1H,1H,2H,2H-perfluorododecyltrichlorosilane [$CF_3(CF_2)_9(CH_2)_2SiCl_3$], also known as FDDTS, was also investigated in this research to achieve even higher degrees of superhydrophobicity. In order to achieve a high degree of hydrophilicity or superhydrophilicity, 3-cyanopropyltrichlorosilane [$CN(CH_2)_3SiCl_3$], also known as CPTS, was selected for the CIT process because of the highly polar −CN group in its chemical structure, which

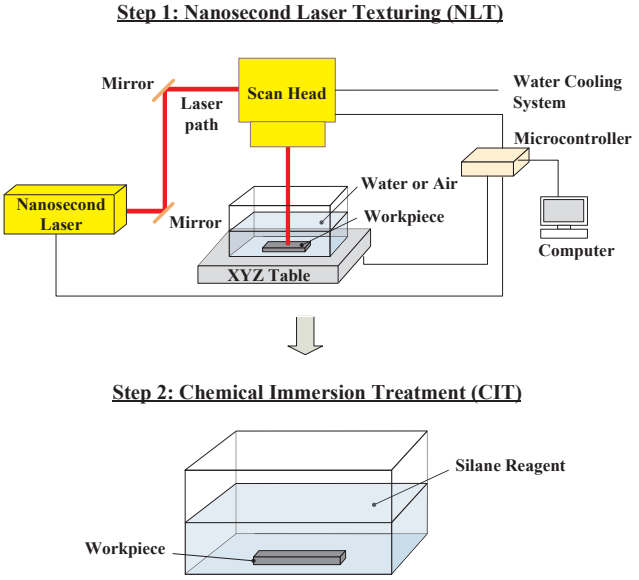

Fig. 2. Process schematic of the nHSN process consisting of two steps: (1) nanosecond laser texturing (NLT) and (2) chemical immersion treatment (CIT).

facilitates the high attractive force for water molecules [46]. The nHSN experiments conducted in this work were only focused on the combination of wNLT and CIT.

A 10,000 mm^2 area AA 6061 specimen treated with the nHSN process is shown in Fig. 3, where spherical water droplets are formed, demonstrating superhydrophobicity when water is sprayed on the surface. For this specimen, a specific laser scanning rate (defined as the area that can be laser processed in a unit time duration of 1 min and indicated by the symbol of R_s) of 13.4 cm^2/min was achieved using the following laser-processing parameters: laser power intensity (I_P) of 0.40 GW/cm^2, pulse energy (E) of 338 mJ, D of 3.7 mm, y-spacing (L_y) of 1.5 mm, overlap ratio (O_r) of 50%, and v of 15 mm/s. It took only ~7.5 min to scan this 100 mm × 100 mm area. It should be noted that the laser-processing rate is still limited in this case due to the laser equipment constraint of the current system using a laboratory laser (Spectra-Physics Quanta-Ray Lab-15 ns laser). An industry-level nanosecond laser will scale up the laser-processing rate and enable a larger area by using a higher laser spot and higher laser repetition rate.

2.2. nHSN experiments

Important processing variables such as target materials, silane reagent, and laser operation parameters were evaluated for their roles in the nanostructuring mechanism and extreme wettability by performing

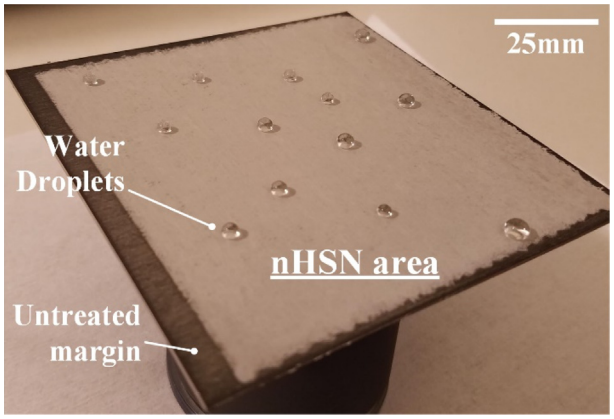

Fig. 3. Spherical water droplets formed on superhydrophobic AA 6061 specimen surface produced by the nHSN process that combines wNLT and CIT. The processed area shown in this figure is 100 mm × 100 mm.

a set of nHSN experiments. Several important engineering alloys were used as work material in this research, including AISI 4130 steel, AA 6061 alloy and Ti-6Al-4V. These engineering alloys have been widely used for a range of applications in the aerospace, marine, power generation and offshore industries. The metal alloy specimens were prepared as ground square sheets. During the NLT experiments, a wide range of laser-processing parameters were evaluated. The processing parameters selected in this work will ensure that the nHSN process can be studied and investigated within a wide processing window, which helps verify the robustness and flexibility of this innovative process. During the CIT treatment, various silane reagents were used to modify the surface chemistry of the laser-textured surfaces. Details about work materials, experimental conditions and chemical reagents are listed in Table 1.

Wetting behaviors of the nHSN specimens were first evaluated using the dynamic impinging test, which captured the dynamic interaction of water with the nHSN treated surface. The dynamic impinging test used a trigger system to generate a pulse signal when a water droplet passed through the laser light. A high-speed imaging system (Fastcam Mini WX100, Photron, with a macro lens, 50 mm Nikkor 1.8D, Nikon) was used to receive the pulse signal, and the transient details of the dynamic droplet impinging process were accurately recorded. By illuminating the droplets using an LED spotlight, high-quality images of impacting droplets were captured. For each test, the image acquisition rate was set at 5000 Hz to achieve good resolution of the dynamics (i.e., spreading, receding and rebounding) of the impacted droplets. Values of static θ_w were measured using a contact angle goniometer (Rame-Hart model 100) coupled with a high-resolution CMOS camera (6–60× magnification, Thor Laboratories). For each θ_w measurement, a 4 μL volume of water was dropped to form a still water droplet on the specimen surface, and its optical shadowgraph was obtained using the CMOS camera. The optical shadowgraph was quantitatively analyzed using the ImageJ software to determine the θ_w for each measurement. Multiple θ_w measurements were performed at various locations on each specimen surface, and the average value of the measurement results was obtained. Water droplet roll-off tests were conducted using an in-house designed roll-off angle ($\theta_{Roll\text{-}off}$) measurement apparatus, which consists of a rotatable stage to hold the nHSN treated surface horizontally and tilts the stage with a resolution of 0.1°. For each $\theta_{Roll\text{-}off}$ measurement, a 4 μL water droplet was micro-pipetted onto the nHSN surface and the stage started rotating until the water droplet rolled off the surface. The critical angle that the water droplet begins to slide down on the inclined stage was recorded as the $\theta_{Roll\text{-}off}$.

The surface topological features generated during the nHSN process were examined by a Hitachi S-4800 SEM. The SEM images were taken at different magnifications ranging from 100× to 20,000× to provide both an overall picture and details (such as ripples, protrusions, pores and cavities at nanoscale) of the generated surface nanostructure.

The surface chemistry of the nHSN treated surface was investigated by XPS using a Kratos Axis Ultra high-performance system. The incident radiation of monochromatic Al Kα X-ray (1486.6 eV) was projected 45° to the sample surface at 150 W (accelerating voltage 15 kV and emission current 10 mA), and the photoelectron data was collected at a takeoff angle of 90°. The chamber pressure was set in the ultra-high vacuum range (10^{-9} torr). Survey scans were taken at a pass energy of 160 eV and conducted over the binding energy range of 1200 eV to 5 eV with an increment step of 1.0 eV and a dwell time of 200 ms. Before the identification of each peak, the whole recorded wide-scan spectrum was aligned with the binding energy of C 1 s to calibrate the binding energies. Core level spectrum analysis was done at a pass energy of 20 eV with an increment step of 1.0 eV and a dwell time of 1000 ms to acquire the detailed distributions of different chemical groups. After the XPS measurements were done, the spectra analyses were conducted using the CasaXPS software.

During the nHSN process, surface nanostructure was generated by combination of NLT and CIT steps. As CIT is critical for inducing the surface chemical etching effect, it is important to understand the extent of the effect during the nHSN process. Therefore, quantitative analysis of the etched-away trace elements was required after the process to determine the etching rate depending on the workpiece material. To validate the surface chemical etching effect, the metal trace elemental concentration of the post-CIT chemical solution was determined using the Varian ICP-OES 720-ES. This technique is a very powerful tool for accurate quantitative chemical analysis [47].

3. Superhydrophobic nHSN treatment

The nHSN superhydrophobic treatment uses fluorosilane reagents such as FOTS and FDDTS for the CIT process. A dynamic impinging test was conducted for the FOTS superhydrophobic treated AA 6061 surface to analyze the dynamic non-wetting behavior. As shown in Fig. 4, at the beginning of the impinging test (t = 0.1 ms), the water mass started to contact the nHSN superhydrophobic surface. At t = 0.5 ms, a rapid spreading process during the water droplet impinging onto the surface was observed. Subsequently, the water droplet rebounded from the surface at t = 5.0 ms. As the water impinged the superhydrophobic surface, the water mass flowed only over the tip of the rough area, while air pockets were trapped underneath the water droplet. Therefore, the capillary force of this process should be quite small, which

Table 1
Experimental conditions for nHSN.

Materials	D (mm)	v (mm/s)	I_P (GW/cm^2)	Chemical reagent
AISI 4130 Steel, AA 6061, Ti-6Al-4V	0.8, 1.0, 1.5, 1.8, 2.0, 2.5, 3.0, 3.3, 3.7, 4.2, 5.2, 6.0, 6.8, 7.2	3.2, 4, 6, 7.2, 8, 10, 12, 13.25, 15, 17, 21, 24, 27.5, 29	0.1, 0.12, 0.15, 0.2, 0.3, 0.4, 0.5, 0.6, 0.9, 1.3, 1.7, 2.4, 5.4, 7.3, 8.4, 11.8, 18.2	1H,1H,2H,2H-perfluorooctyltrichlorosilane $[CF_3(CF_2)_5(CH_2)_2SiCl_3]$ (FOTS; 98%) 1H,1H,2H,2H-perfluorododecyltrichlorosilane $[CF_3(CF_2)_9(CH_2)_2SiCl_3]$ (FDDTS; 97%) 3-Cyanopropyltrichlorosilane $[CN(CH_2)_3SiCl_3]$ (CPTS; 97%)

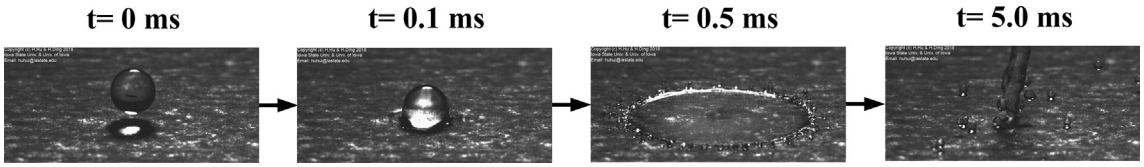

Fig. 4. Dynamic impinging test for nHSN treated superhydrophobic AA 6061 surface.

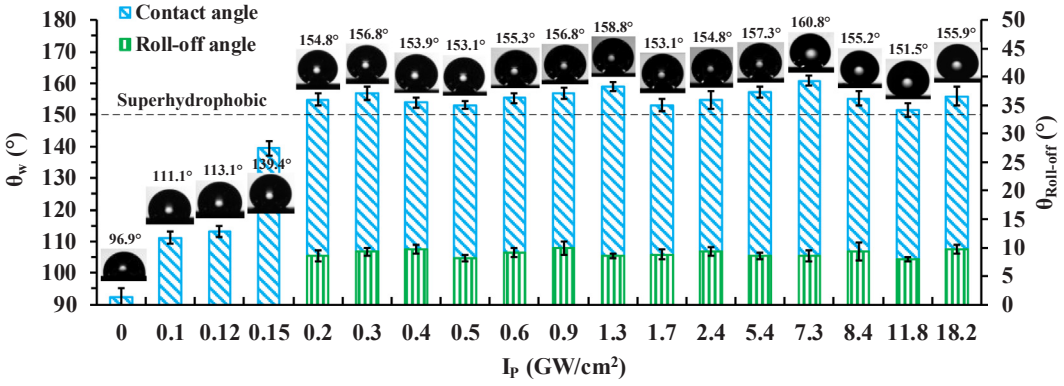

Fig. 5. Water contact angle and roll-off angle measurement results for nHSN superhydrophobic treatment of AISI 4130 steel.

would lead to a large receding velocity due to the low water movement resistance. The upward rebounding phenomenon of the water mass was thus observed as a result of the low resistance.

3.1. Superhydrophobic surface characterization

The effect of laser power intensity was evaluated through the nHSN experiments using the same silane reagent FOTS. For AISI 4130 steel specimens, laser power intensity I_P varied from 0 to 18.2 GW/cm^2, with zero indicating no wNLT treatment and only CIT treatment. θ_w for all these process conditions is plotted in Fig. 5, and the measurement uncertainty in θ_w is within ± 2° for each condition. For I_P of 0 GW/cm^2, a θ_w of 96.9° demonstrates that the CIT process alone is not sufficient to achieve superhydrophobicity. The specimens treated by a low I_P, ranging from 0.1 to 0.15 GW/cm^2 during the nHSN process, show improved surface hydrophobicity with θ_w increased to 139.4°. These tests also indicate that a higher I_P during wNLT helps increase the θ_w achieved by the nHSN process. The specimens treated by an I_P ranging from 0.2 to 18.2 GW/cm^2 during the nHSN process achieve superhydrophobicity with θ_w greater than 150°. Therefore, the threshold I_P value for AISI 4130 steel is 0.2 GW/cm^2, which ensures superhydrophobicity can be achieved using the nHSN process when an I_P higher than the threshold value is used. Varying I_P does not significantly alter the θ_w for these superhydrophobic AISI 4130 steel specimens. These results indicate that a wide laser operation window exists for the nHSN process and can produce consistent superhydrophobic AISI 4130 steel surfaces, as long as the I_P is equal to or greater than 0.2 GW/cm^2.

For AA 6061, I_P varied from 0 to 8.4 GW/cm^2, and the θ_w measurement results can be found in Fig. 6. Similarly, the measurement variation of θ_w was typically around ± 2° for each test. An untreated AA 6061 specimen that went through CIT only shows a θ_w of 92.3°. The specimens treated by a low I_P ranging from 0.2 to 0.3 GW/cm^2 during the nHSN process showed an improvement in hydrophobicity, with θ_w increased to 133.8°. If the I_P value is increased to 0.4 GW/cm^2 or higher, superhydrophobicity can be achieved on AA 6061. The θ_w measurement results for both materials indicate that the nHSN process is very robust and flexible. The threshold value of I_p to achieve superhydrophobicity also varies based on the work material. This wettability analysis for both of the materials indicates that not only a wide range of process window for superhydrophobicity but also a tunability of hydrophobicity from 90° to 160° can be realized by controlling the laser power intensity.

To further validate the superhydrophobicity achieved on the nHSN treated AISI 4130 and AA 6061 surfaces, the $\theta_{Roll\text{-}off}$ of both surfaces was characterized during the water sliding tests. The experimental results demonstrate that the $\theta_{Roll\text{-}off}$ for both nHSN treated surfaces are between 8°-10° with an uncertainty of 0.8° within the above-mentioned I_P range. For a typical superhydrophobic surface, θ_w is usually above 150° and $\theta_{Roll\text{-}off}$ is generally below 10° [48]. The $\theta_{Roll\text{-}off}$ measurement results further demonstrate the effectiveness of the nHSN process to produce consistent superhydrophobic surfaces within a wide laser operation window.

The effects of fluorosilane reagents were also studied for the superhydrophobic nHSN treatment. The difference of two fluorosilane reagents, namely FOTS and FDDTS, is the length of the $-CF_2-$ chain in the functional group in their chemical structure. FOTS has the lower length of the $-CF_2-$ chain while FDDTS has the higher length of the $-CF_2-$ chain. A superhydrophobic nHSN treatment was conducted on two different materials, namely Ti-6Al-4V and AA 6061. The comparison of the θ_w measurement results is shown in Fig. 7. Ti-6Al-4V is only highly hydrophobic when chemically treated using FOTS. However, it becomes superhydrophobic when it is treated with FDDTS. For AA 6061, the θ_w is above 150° for both I_P values. However, the θ_w value is increased when the length of the functional group is increased. These experimental results clearly illustrate the influence of the length of the functional group on the surface superhydrophobicity. The longer the silane tail group length, the higher the θ_w. This finding shows that controlling the surface chemistry is primarily critical to modify the surface wetting behavior for the nHSN processes.

3.2. Surface nanostructuring

nHSN surface topological structures were evaluated using an SEM micrograph analysis. Fig. 8k shows a typical high-magnification (20,000×) SEM micrograph for an AISI 4130 steel surface processed using an nHSN superhydrophobic treatment, which is characterized by random nanostructures of various protrusions and cavities, ranging in size from less than 100 nm to several hundred nm, randomly and closely packed in the treated area. At relatively low magnifications (Fig. 8i and j) with a view area of about 1 mm^2, the nHSN specimen exhibits an isotropic texture with numerous tiny pores homogenously distributed in

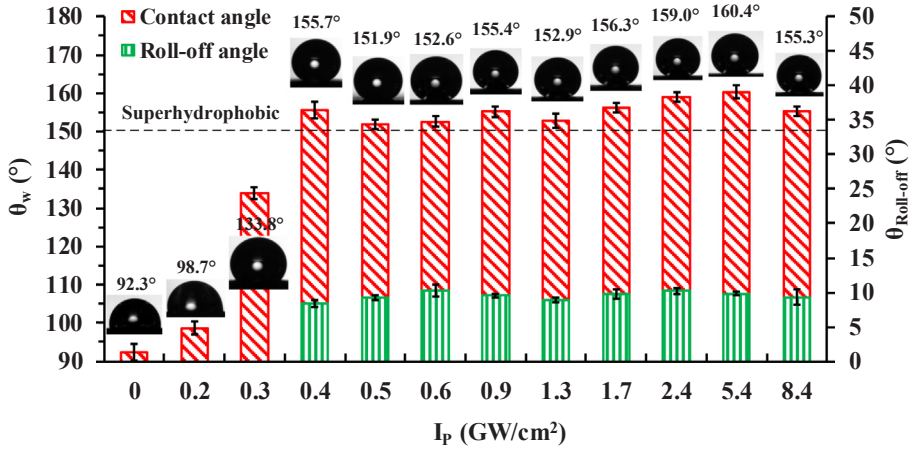

Fig. 6. Water contact angle and roll-off angle measurement results for nHSN superhydrophobic treatment of AA 6061.

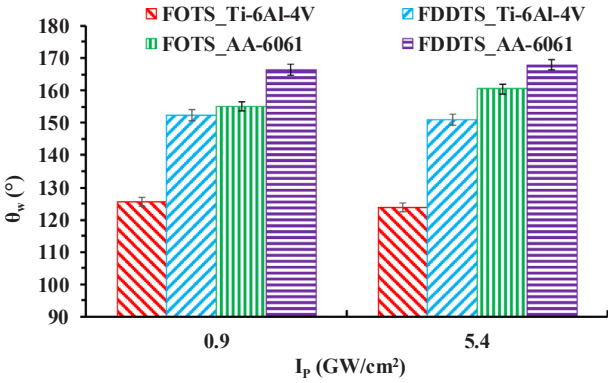

Fig. 7. Comparasions of FOTS and FDDTS silane reagents on nHSN superhydrophobic treatment.

the treated area, but no obvious microscale patterns can be observed. The random surface nanostructures generated from nHSN are fundamentally different from those manufactured by existing ultrashort laser-based surface-texturing methods, which take the top-bottom approach and often rely on the generation of LIPSS (see Fig. 8a [49]) or micro-scale patterns (see Fig. 8b [37]) over the area. The ultrashort laser-based surface-texturing methods scan the surface area using a focused laser spot (often in the range of 30–50 μm) and a very fine spatial resolution. Hence, the resultant surface topological features are very structured in the local area. In contrast, the NLT phase of nHSN uses a large laser spot and high scanning speed to scan and precondition the surface, while the whole macroscale area is nanostructured with dense nanoscale features from the CIT phase.

Fig. 8c–k compares the progression of the surface topology of AISI 4130 steel from the untreated raw material condition to the wNLT and nHSN conditions. These SEM analyses of AISI 4130 steel, as well as other metal alloys, clearly support the occurrence of surface nanostructuring resulting from chemical etching due to a reaction between the laser-textured metal surface and the chlorosilane reagent during CIT. The untreated surface exhibits a horizontal lay pattern at various magnifications, as shown in Fig. 8c–e. Without the CIT treatment, the

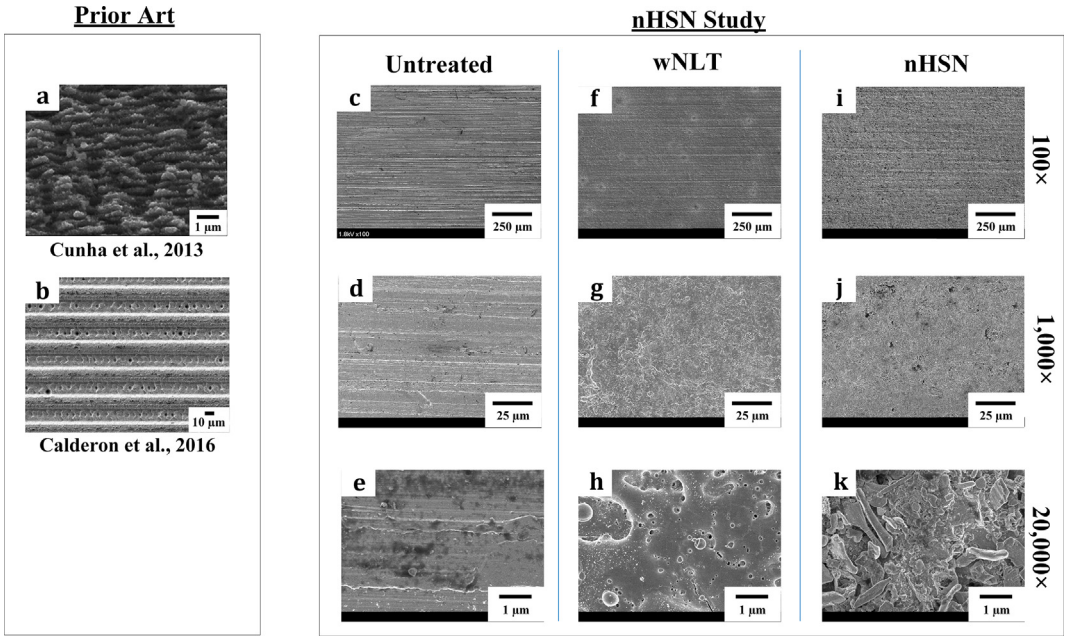

Fig. 8. SEM images of (a–b) superhydrophobic surface structures produced by the existing femtosecond laser-texturing techniques. (a) is reproduced from Cunha et al. [41] and (b) is reproduced from Martínez-Calderon et al. [37]; (c–e) untreated surface; (f–h) wNLT surface; (i-k) nHSN surface on AISI 4130 steel processed using the I_P of 7.3 GW/m^2.

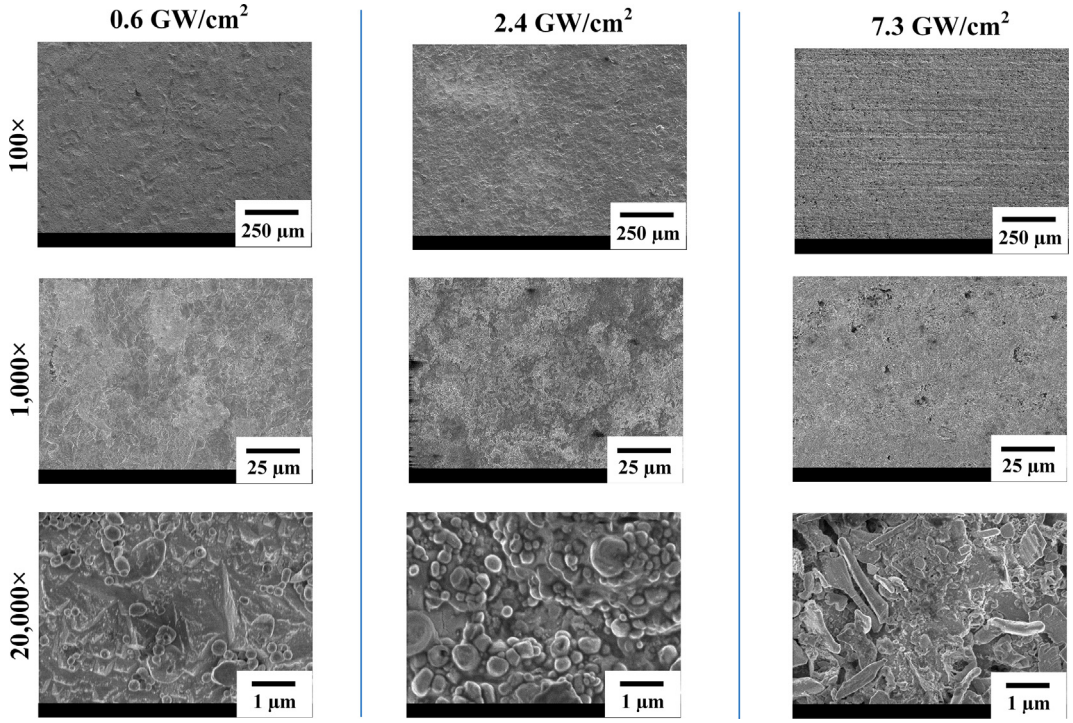

Fig. 9. SEM micrographs of nHSN superhydrophobic AISI 4130 steel surfaces processed using various I_P.

wNLT laser-textured surface is characterized by microscale surface ripples, is dispersed with pores (Fig. 8f–h) and is hydrophilic. The distinct difference between the wNLT surface and nHSN surface clearly supports the occurrence of surface nanostructuring resulting from chemical etching due to the reaction between the laser-textured metal surface and the fluorosilane FOTS reagent during the CIT step. The chemical etching mechanism will be examined in the following section.

Although not the most critical factor in the nanostructuring mechanism, the laser power intensity I_P used during wNLT affects the feature size and distribution of surface nanostructure during the CIT phase. nHSN specimens treated using different I_P were examined using SEM, as shown in Fig. 9. At 20,000× magnification with a view area of about 20 μm^2, random structures of various shapes of protrusions, rods, cones, platelets, and pores are revealed for all these nHSN specimens. In comparison with the surfaces treated at the I_P of 0.6 GW/cm^2 and 2.4 GW/cm^2, a higher I_P of 7.3 GW/cm^2 during wNLT induces more significant surface nanostructuring effects during the subsequent CIT phase, resulting in a feature size decrease and an increase in nanoscale feature density. This illustrates that the I_P during the NLT phase can be used to finely tune the surface nanostructure during the CIT phase.

3.3. Superhydrophobic surface chemistry

The surface chemistry of the nHSN surface is the key factor for achieving desired surface wettability. In this section, the surface chemistry of the untreated surface, wNLT surface and nHSN surface chemically treated using FOTS for AA 6061 were quantitively analyzed by XPS. The XPS survey spectra taken on the surface layer of the different surfaces can be found in Fig. 10, and the detailed elemental composition on the surface layer can be detected. For the untreated surface, elements such as aluminum, magnesium, oxygen and carbon could be detected on the surface, as shown in Fig. 10a. It can be observed that immediately after wNLT, the same elements were detected on the laser-textured surface. The aluminum and magnesium came from the substrate material, and the oxygen came from the oxidation/hydroxylation that occurred during wNLT (Fig. 10b). For the sample that went through both wNLT and a subsequent CIT process, a significantly different XPS spectrum was observed. Two additional peaks in fluorine and silicon along with oxygen, carbon and aluminum were observed in the survey spectrum at the surface layer (Fig. 10c). The source of the fluorine and silicon belonged to the FOTS reagent [$CF_3(CF_2)_5(CH_2)_2SiCl_3$]. Core-level analysis of the carbon element shows that the carbon peak is a combination of the $-CH_2-$, $-CF_2-$ and $-CF_3$ chemical groups (Fig. 10c). Those functional groups are present on the FOTS structure, which indicates that the FOTS molecules are successfully attached to the CIT treated surface, leading to surface fluorination. Researchers have shown that presence of $-CF_2-$ and $-CF_3$ groups on the surface leads to low surface energy [41,45]. This work also clearly showed that the functional groups were attached to the surface layer of the nHSN superhydrophobic surface. Therefore, the surface energy of the nHSN superhydrophobic surface was significantly reduced, which contributed to the superhydrophobicity. Surprisingly, there was no chlorine signal detected in the XPS survey spectrum, although there were three chlorine atoms in the chemical structure of the FOTS reagent. This is because the chlorine atoms reacted with the metal substrate during the CIT process and dissolved in the chemical solution as metal chloride after being chemically etched.

To explore the extent of etching effects during the nHSN process, the metal trace elemental concentration of the post-CIT chemical solution was obtained by ICP-OES experiments to determine the etching rate during the nHSN treatment. This technique provides accurate quantitative chemical analysis. The chemical solutions that remained after the CIT process of the superhydrophobic AA 6061 and AISI 4130 specimens were collected, and ICP-OES analysis was conducted using these solutions. The schematic representation of the experimental setup for ICP-OES analysis is shown in Fig. 11a. The solution is converted into a mist of finely divided droplets (aerosol) through nebulization and introduced to the plasma chamber. The plasma excites the atoms, which leads to light radiation. The radiated light is separated into different wavelengths in the grating chamber. Subsequently, the semiconductor photodetector measures the intensity of each wavelength, which allows the detection of trace elements present in the solution. The wavelength of the radiated light from Fe and Al elements are 238.204 nm and 396.152 nm, respectively. The analysis shows that the post-CIT-process

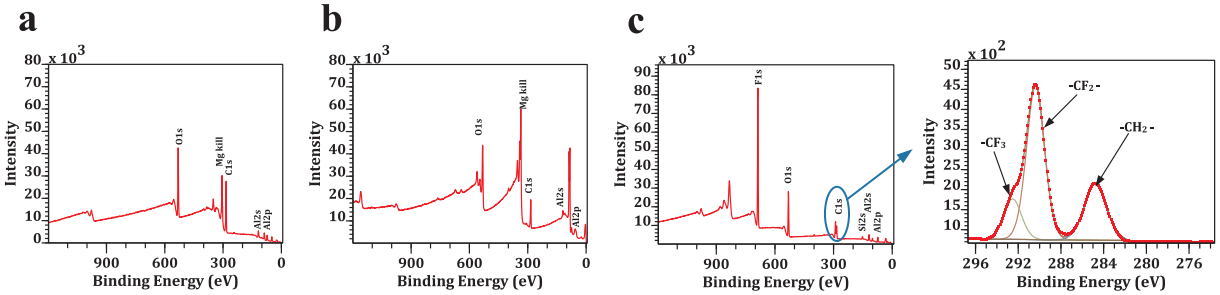

Fig. 10. XPS survey spectra of the surface layer for AA 6061: (a) untreated surface; (b) wNLT surface and (c) nHSN surface chemically treated with FOTS reagent.

solution for AISI 4130 steel has a strong intensity peak for the Fe trace element, whereas only the FOTS solution required for the CIT process does not have any intensity peak (Fig. 11b). A similar result is observed for the post-CIT-process solution of AA 6061, where a strong intensity peak of the Al trace element is observed, while no intensity peak is detected for the FOTS-only solution. This proves that the CIT process induces a significant etching effect that brings the Fe element and the Al element from the AISI 4130 steel and the AA 6061 substrate, respectively, into the chemical solutions. It also validates the hypothesis that the cholerine reacted with the metal substrate and etched away the metal atoms from the surface. The etched metal eventually dissolves into the solution as metal chloride.

3.4. Discussions

Based on these detailed SEM, XPS and ICP-OES analyses, there are several key findings for the nHSN process mechanisms:

- The nHSN surface exhibits a unique surface structure consisting of random nanostructures of various protrusions and cavities ranging from several tens to several hundreds of nm. These surface structures are fundamentally different from those in the existing literature.
- Very complex chemical reactions, including surface chemical etching, fluorination, oxidation and hydroxylation, are believed to take place simultaneously between the laser-textured metal surface and the fluorosilane reagent during the CIT process. This should be considered as one of the key findings and is quite different from what has been claimed in previous studies, which is that only surface fluorination occurs on the laser-textured surface during the chemical treatment [14,15]. The chemical etching event is the key reason behind the nanostructure generation during the CIT process, as shown in Fig. 8.
- Low energy functional groups, namely the $-CF_2-$ and $-CF_3$ groups, were found to be attached to the nHSN surface. These groups reduce the surface energy and contribute to the surface wettability change.
- The reagents used to achieve superhydrophobicity have reactive group [$-SiCl_3$] with three chlorine atoms on each molecule and functional groups with $-CF_2-$ and $-CF_3$. These chlorine atoms react with the surface hydroxide of the laser textured surface. During this reaction process, three molecules of HCl are generated corresponding to each molecule of the reagent. These HCl molecules were responsible for the etching effect which helps to generate the final nanostructure during the CIT process. The occurrence of the etching effect was confirmed by the ICP-OES analysis as shown in Fig. 11. In the meantime, successful attachment of functional groups also happened during the CIT process, which is confirmed by the XPS analysis as shown in Fig. 10. This indicates a simultaneous generation of nanostructure and surface chemistry during the CIT process.
- It is also observed that increasing the I_P during the nHSN process will generate a higher density of random surface nanostructures. This demonstrates that control of laser-processing parameters can be used to finely tune the surface nanostructure.

Based on these findings, it is believed that the random surface nanostructure generated during the nHSN process and the surface chemistry change leading to surface energy reduction are both key factors for the significant improvement in wettability. Therefore, the surface chemistry and surface structure of the nHSN surface should be considered equally critical for achieving the target wettability condition. These new findings are believed to be an important part of the new material processing sciences discovered in this work and will provide critical insights for the interdependence of laser texturing and surface chemistry modification and how to control the nHSN process.

4. Superhydrophilic nHSN treatment

The nHSN superhydrophilic treatment uses cyanosilane reagents such as CPTS for the CIT process. The surface wettability change, surface features and surface chemistry for the superhydrophilic/highly hydrophilic surface fabricated by the nHSN process are investigated and analyzed in this section. nHSN experiments were conducted for AISI

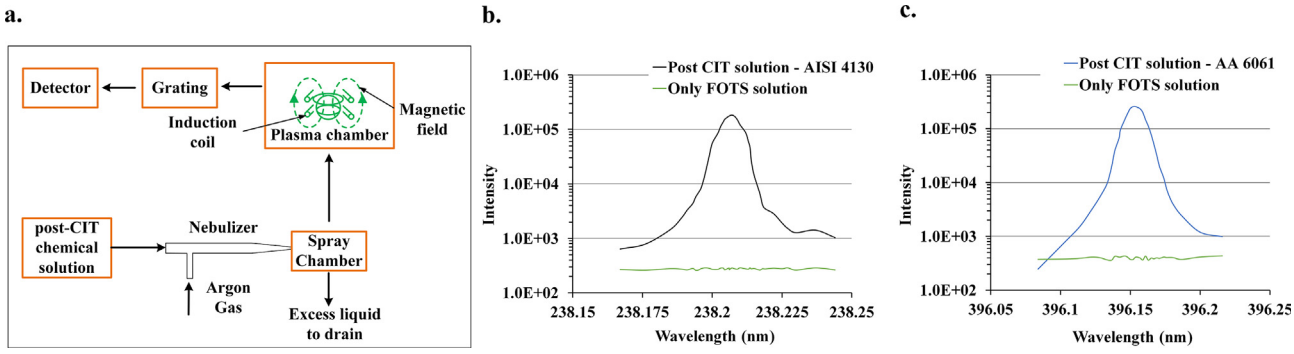

Fig. 11. (a) Schematic representation of the experimental setup for ICP-OES analysis; (b) comparison of intensity plot of Fe trace element between pure FOTS solution and post-CIT-process solution of AISI 4130 steel; and (c) comparison of intensity plot of Al trace element between pure FOTS solution and post-CIT-process solution of AA 6061.

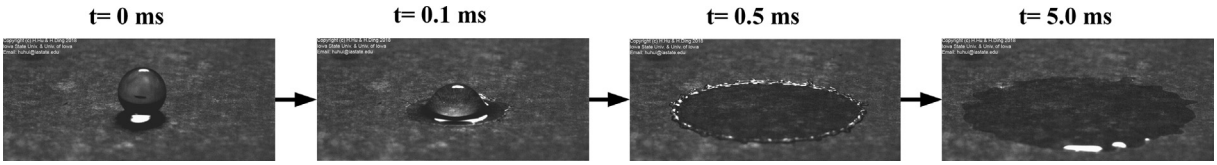

Fig. 12. Dynamic impinging test for nHSN superhydrophilic AA 6061 surface.

4130 steel and AA 6061 using a CPTS [$CN(CH_2)_3SiCl_3$] reagent. The dynamic wetting behavior of the nHSN superhydrophilic surface was characterized via a dynamic impinging test as shown in Fig. 12. When the droplet impinged on the superhydrophilic surface, the water mass started to spread on the surface, as shown at the time step of t = 0.1 ms. During the water spreading, water beads were found to form along the rim of the outer ring of the impinged water droplet, which can be seen at the time step of t = 0.5 ms. The surface has a high affinity for water due to the polar surface chemistry. Therefore, the large polar-polar attraction force suppresses the receding movement. The impinged water droplet then reached its maximum spread diameter at the time step of t = 5.0 ms, and no receding process occurred. A water film was formed over the superhydrophilic surface after the impinged water mass reached the steady-state.

4.1. Superhydrophilic surface characterization

The variation of hydrophilicity with respect to the laser power intensity is investigated in this section. I_P varied from 0.1 GW/cm^2 to 8.4 GW/cm^2 in the wNLT process. The variation of θ_w for AISI 4130 steel with respect to I_P is shown in Fig. 13a. The θ_w for the AISI 4130 specimen treated with the CIT process only is slightly higher than 90°. This indicates that the CIT process alone could not achieve superhydrophilicity. The specimens treated with a low I_P ranging from 0.1 to 0.4 GW/cm^2 during wNLT show a θ_w between 30° and 90°. These tests indicate that a higher I_P helps to decrease the θ_w during the nHSN process. A further increase in I_P during the wNLT process improved the θ_w to the superhydrophilic range ($\theta_w < 10°$). All the specimens treated by an I_P ranging from 0.5 to 8.4 GW/cm^2 achieve superhydrophilicity with a θ_w less than 10°. These results indicate that a superhydrophilic AISI 4130 steel surface could be produced, as long as the I_P was equal to or greater than 0.5 GW/cm^2.

A similar experimental analysis was conducted on AA 6061, and the corresponding results are shown in Fig. 13b. The CIT treatment on untreated AA 6061 only leads to a θ_w of 95°. For an I_P ranging from 0.2 GW/cm^2 to 0.5 GW/cm^2, the θ_w is reduced from 90° to 60° as the I_P increases. These tests also indicate that a higher I_P helps to decrease the θ_w during the nHSN process. A further increase in I_P significantly reduces the θ_w to the highly hydrophilic range. All the specimens treated by I_P ranging from 0.6 to 8.4 GW/cm^2 achieved superhydrophilicity with a θ_w of 10° or high degrees of hydrophilicity with a θ_w less than 30°. These results indicated that highly hydrophilic AA 6061 surfaces could be produced, as long as the I_P was equal to or greater than 0.6 GW/cm^2. The experimental results indicate that the nHSN process has a wide process window for the fabrication of a superhydrophilic/highly hydrophilic surface and that the surface hydrophilicity can also be tuned by controlling the laser power intensity. Care also must be taken when selecting the laser parameter to control the resultant surface hydrophilicity for different materials.

4.2. Surface nanostructuring

The surface microstructures produced by the nHSN superhydrophilic treatment were analyzed at different magnifications, as illustrated in Fig. 14. The specimens were processed using an I_P of 0.6 GW/cm^2 and 8.4 GW/cm^2. The nHSN superhydrophilic specimens show an isotropic texture at 100× magnification. At 1,000× magnification, spherical nanostructures are homogeneously distributed on the processed surfaces, but it is difficult to distinguish the feature size. Images at the magnification of 20,000× clearly show that the processed surfaces consist of spherical nanostructures with the feature size ranging from a few tens to a few hundreds of nanometers. Although the surface structures of the nHSN superhydrophilic surface are not identical to those of the nHSN superhydrophobic surface, the nHSN treatment using the CPTS reagent shows its effectiveness in the generation of surface nanostructures. The SEM analysis for the nHSN superhydrophobic/superhydrophilic surface confirms that the nHSN process is a very robust and flexible surface nanostructuring process, regardless of which chemical reagent is used.

4.3. Hydrophilic surface chemistry

The surface chemistry of the untreated surface, the wNLT surface and the nHSN surface chemically treated using CPTS were also quantitively analyzed by XPS, as illustrated in Fig. 15. The elemental compositions for the untreated surface and the NLT surface here are found to be identical to those in Section 3.3, as the materials and laser-processing parameters used are the same, as shown in Fig. 15a and b. However, the nHSN surface that went through CIT using the CPTS reagent exhibits a significantly different XPS spectrum compared to that of the nHSN surface chemically treated using the FOTS reagent. Two additional peaks in nitrogen and silicon along with oxygen, carbon and aluminum were observed in the survey at the nHSN highly hydrophilic surface, as shown in Fig. 15c. The elements of nitrogen and silicon originate from the CPTS reagent [$CN(CH_2)_3SiCl_3$]. There are two functional groups, namely the −CN and $-CH_2-$ groups, present on the CPTS structure. The source of nitrogen and silicon is the CPTS reagent [$CN(CH_2)_3SiCl_3$]. The −CN and $-CH_2-$ groups present on the CPTS structure were attached to the laser-textured surface leading to the surface nitriles group. The nitriles group is known to be hydrophilic because of the highly polar −CN covalent bond. Therefore, with its attachment to the surface, the processed surface behaves as highly hydrophilic. Through the SEM and XPS analyses of the nHSN highly hydrophilic surface, it is confirmed that a nanostructured metal surface with cyano-silane chemistry is water attractive.

An ICP-OES analysis was also conducted on the post-process solution of the CIT process with the CPTS reagent. The result demonstrates that the chemical etching event also occurred during the CIT process using the CPTS reagent, which is similar to that using the FOTS reagent.

5. Process throughput analysis

A process throughput analysis was conducted to compare the processing efficiencies of this innovative nHSN process and the existing laser-based surface-texturing methods. Existing laser-based surface-texturing methods often use ultrashort pulsed lasers, i.e., femtosecond or picosecond pulsed lasers, for fabrication of the superhydrophobic or superhydrophilic surfaces. These methods generate the periodic nanoscale features and scan the material surface at a very fine spatial resolution with extremely low process throughput. These methods also use various post-laser treatments, as discussed in the introduction section, to reduce the surface energy of the laser-textured surfaces. The process throughput of the existing laser-based processes is limited mainly due to the low laser surface-texturing rate. In this work, only the

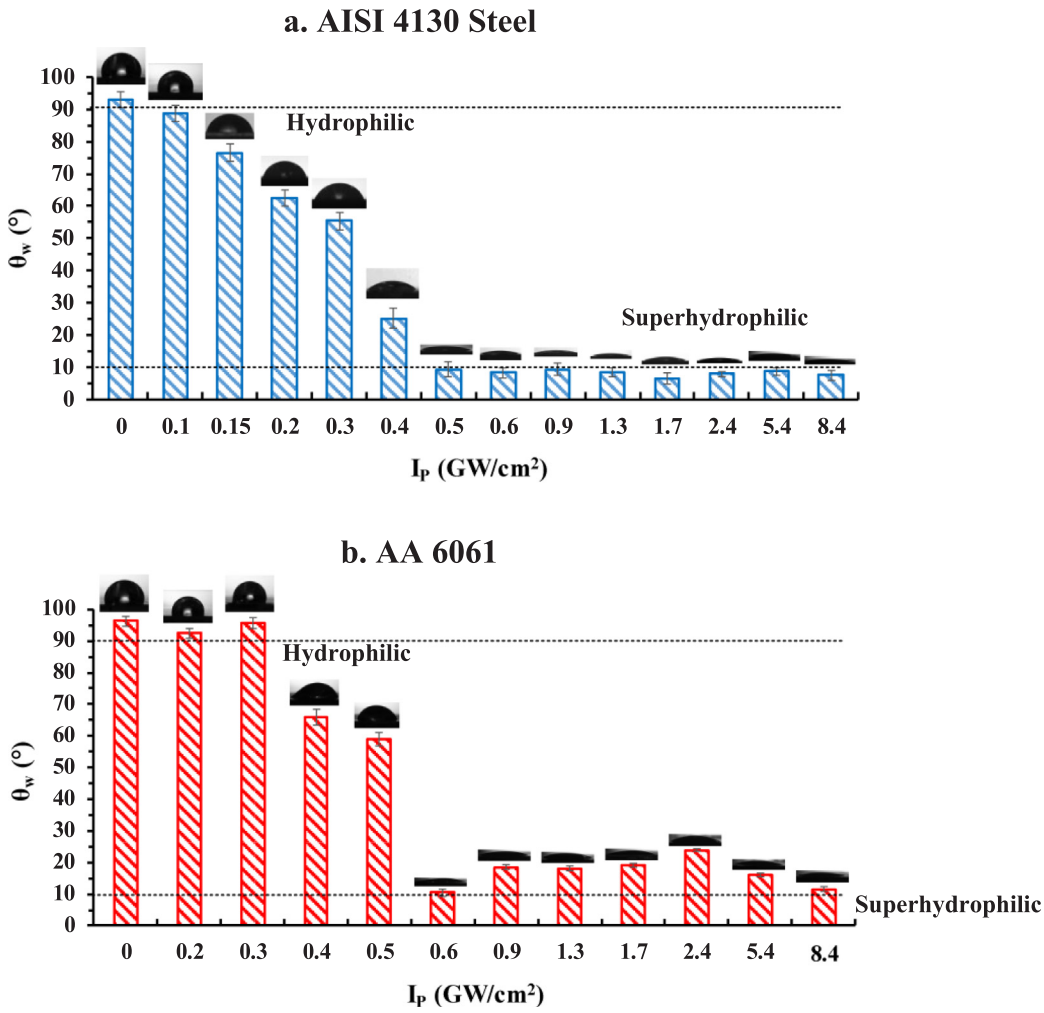

Fig. 13. θ_w measurement results for (a) nHSN AISI 4130 steel and (b) nHSN AA 6061 specimens produced by the wNLT process at various I_P ranging from 0 to 8.4 GW/cm^2 followed by CIT process using CPTS reagent.

laser surface-texturing rate during the wNLT step is discussed and compared with the existing laser-texturing methods.

In the throughput analysis of laser texturing, the main parameter to be discussed is R_s, i.e., the area that can be laser processed in a unit time duration of 1 min. The higher the R_s is, the higher the process throughput. The R_s using the nHSN process and other existing laser-based surface-texturing methods is as shown in Fig. 16. For the nHSN process, an R_s of 51.6 cm^2/min can be achieved using the following laser-processing parameters: I_P of 0.20 GW/cm^2, E of 710 mJ, D of 7.5 mm, L_y of 3 mm, O_r of 50% and v of 30 mm/s. An industry-level nanosecond laser will further scale up the laser-processing rate and enable a larger area by using a higher E and a higher f while

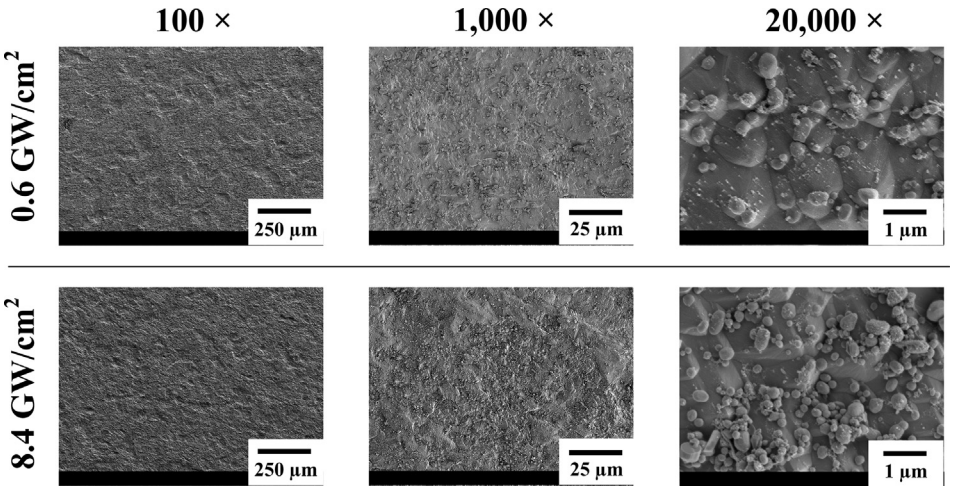

Fig. 14. SEM images of nHSN superhydrophilic surfaces fabricated on AISI 4130 steel using I_P of 0.6 GW/cm^2 and 8.4 GW/cm^2.

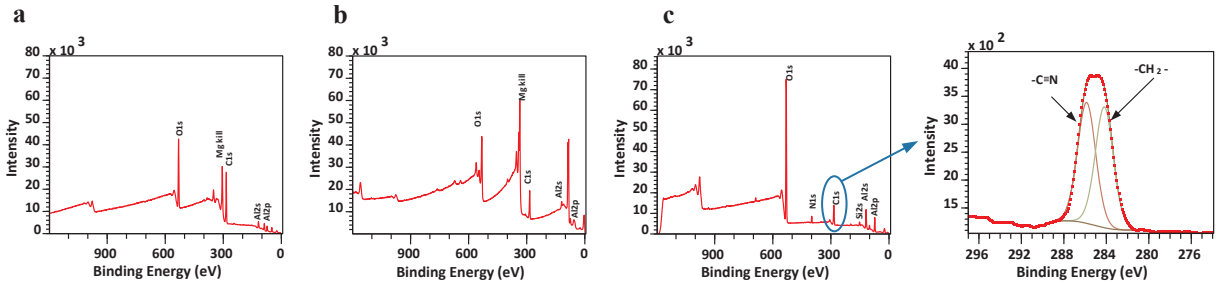

Fig. 15. XPS survey spectra of the surface layer for AA 6061: (a) untreated surface; (b) wNLT surface and (c) nHSN surface chemically treated with CPTS reagent.

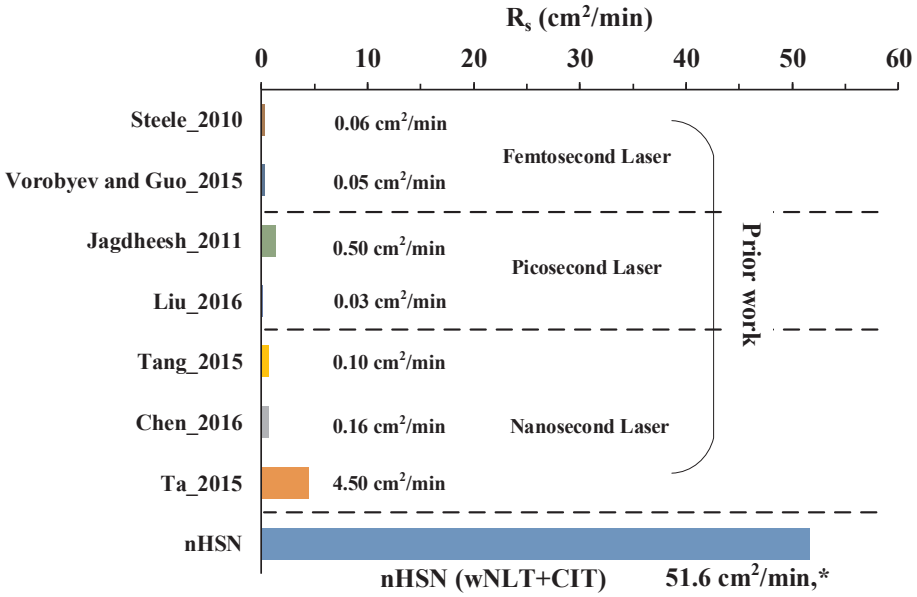

Fig. 16. R_s for nHSN process and other existing laser-based surface-texturing methods. * It should be noted that the R_s calculation for the nHSN process discussed in this work is based on a laboratory laser (Spectra-Physics Quanta-Ray Lab-15 ns laser). An industry-level nanosecond laser will further scale up the laser-processing rate.

maintaining the same I_P. However, the R_s is much lower for the other existing laser-based surface-texturing methods. For femtosecond laser surface-texturing methods, the R_s is on the level of 0.05–0.06 cm^2/min with the data obtained from research papers by Vorobyev and Guo [20] and Steele et al. [43]. For picosecond laser surface-texturing methods, the R_s is on the level of 0.03–0.5 cm^2/min with the data obtained from research papers by Jagdheesh et al. [22] and Liu et al. [21]. For nanosecond laser surface-texturing methods, the R_s is on the level of 0.1–4.5 cm^2/min with the data obtained from research papers by Tang et al. [44], Chen et al. [41] and Ta et al. [26]. It is found that the nHSN process is at least one order faster than the existing laser-based surface-texturing methods. It can thus be concluded that, compared with the existing ultrashort laser-based surface-texturing techniques, the nHSN process significantly increases the processing rate and thus will enable large-area processing for practical throughput.

6. Conclusions

- A novel nHSN process was developed that is capable of efficiently creating high-density nanostructures over large metal alloy surface areas and attaining desired surface chemistry for extreme wettability applications.
- The mechanism of surface nanostructuring by the nHSN process is fundamentally new, which results from a combined effect of chemical etching and attachment of functional groups during the CIT phase of nHSN.
- Based on the new nanostructuring mechanism, the proper silane reagent can be selected for the CIT phase to achieve the desired surface wetting behavior, while laser parameters can also be adjusted during the NLT phase to finely tune the nanostructuring mechanism.
- Extreme wettability including superhydrophobicity and superhydrophilicity is demonstrated for multiple engineering metal alloys, including aluminum, steel and titanium alloys.
- Compared with the existing ultrashort laser-based surface-texturing techniques, the nHSN process significantly increases the laser-processing rate by at least two orders and greatly reduces the production cost, which will enable large-area processing of engineering alloys for practical throughput.

These new findings are very important for understanding the interdependence of laser texturing and surface chemistry modification and provide new opportunities for the area of laser surface nanostructuring.

CRediT authorship contribution statement

Qinghua Wang: Conceptualization, Methodology, Investigation, Formal analysis, Visualization, Writing - original draft. **Avik Samanta:** Conceptualization, Methodology, Investigation, Formal analysis, Visualization, Writing - original draft. **Scott K. Shaw:** Resources, Supervision. **Hui Hu:** Resources, Supervision. **Hongtao Ding:** Conceptualization, Methodology, Resources, Supervision, Writing - review & editing, Project administration, Funding acquisition.

Declaration of Competing Interest

The authors declare that they have no known competing financial

interests or personal relationships that could have appeared to influence the work reported in this paper.

Acknowledgements

The authors also would like to acknowledge Majid H. Nada and Prof. Sarah C. Larsen from the Department of Chemistry at the University of Iowa for their help with the ICP-OES experiments, Dr. Joun Lee and Kenny Horkley for their help with XPS measurements, and Prof. Fatima Toor for her useful discussions of this work.

Funding

The authors gratefully acknowledge financial support from the National Science Foundation under Grant Number CMMI-1762353.

References

[1] A.Y. Vorobyev, V.S. Makin, C. Guo, Periodic ordering of random surface nanostructures induced by femtosecond laser pulses on metals, J. Appl. Phys. 101 (2007), https://doi.org/10.1063/1.2432288.
[2] J. Long, Z. Cao, C. Lin, C. Zhou, Z. He, X. Xie, Formation mechanism of hierarchical Micro- and nanostructures on copper induced by low-cost nanosecond lasers, Appl. Surf. Sci. 464 (2019) 412–421, https://doi.org/10.1016/j.apsusc.2018.09.055.
[3] E.A. Bogoslov, M.P. Danilaev, S.A. Mikhailov, Y.E. Pol'skii, Energy efficiency of an integral anti-ice system based on fluoroplastic films, J. Eng. Phys. Thermophys. 89 (2016) 815–820, https://doi.org/10.1007/s10891-016-1441-5.
[4] J.W. Gose, K. Golovin, A. Tuteja, S.L. Ceccio, M. Perlin, Experimental investigation of turbulent skin-friction drag reduction using superhydrophobic surfaces, 31st Symp Nav. Hydrodyn, 2016, pp. 11–16.
[5] R. Jagdheesh, M. Diaz, J.L. Ocaña, Bio inspired self-cleaning ultrahydrophobic aluminium surface by laser processing, RSC Adv. 6 (2016) 72933–72941, https://doi.org/10.1039/C6RA12236A.
[6] K. Ellinas, D. Kefallinou, K. Stamatakis, E. Gogolides, A. Tserepi, Is there a threshold in the antibacterial action of superhydrophobic surfaces? ACS Appl. Mater. Interfaces 9 (2017) 39781–39789, https://doi.org/10.1021/acsami.7b11402.
[7] S. Ji, P.A. Ramadhianti, T.B. Nguyen, W.D. Kim, H. Lim, Simple fabrication approach for superhydrophobic and superoleophobic Al surface, Microelectron. Eng. 111 (2013) 404–408, https://doi.org/10.1016/j.mee.2013.04.010.
[8] M. Paulose, H.E. Prakasam, O.K. Varghese, L. Peng, K.C. Popat, G.K. Mor, T.A. Desai, C.A. Grimes, TiO_2 nanotube arrays of 1000 μm length by anodization of titanium foil: Phenol red diffusion, J. Phys. Chem. C 111 (2007) 14992–14997, https://doi.org/10.1021/jp075258r.
[9] Y. Cai, L. Lin, Z. Xue, M. Liu, S. Wang, L. Jiang, Filefish-inspired surface design for anisotropic underwater oleophobicity, Adv. Funct. Mater. 24 (2014) 809–816, https://doi.org/10.1002/adfm.201302034.
[10] A. Dramé, T. Darmanin, S.Y. Dieng, E.T. De Givenchy, F. Guittard, Superhydrophobic and oleophobic surfaces containing wrinkles and nanoparticles of PEDOT with two short fluorinated chains, RSC Adv. 4 (2014) 10935–10943, https://doi.org/10.1039/c3ra47479h.
[11] A.K. Kota, A. Tuteja, Superoleophobic surfaces, ACS Symp. Ser. 1106 (2012) 171–185, https://doi.org/10.1021/bk-2012-1106.ch011.
[12] Y. Li, X. Zhu, X. Zhou, B. Ge, S. Chen, W. Wu, A facile way to fabricate a super-amphiphobic surface, Appl. Phys. A Mater. Sci. Process. 115 (2014) 765–770, https://doi.org/10.1007/s00339-014-8438-8.
[13] T. Sun, G. Wang, H. Liu, L. Feng, L. Jiang, D. Zhu, Control over the wettability of an aligned carbon nanotube film, J. Am. Chem. Soc. 125 (2003) 14996–14997, https://doi.org/10.1021/ja038026o.
[14] B. Jia Li, H. Li, L. Jing Huang, N. Fei Ren, X. Kong, Femtosecond pulsed laser textured titanium surfaces with stable superhydrophilicity and superhydrophobicity, Appl. Surf. Sci. 389 (2016) 585–593, https://doi.org/10.1016/j.apsusc.2016.07.137.
[15] B. Wu, M. Zhou, J. Li, X. Ye, G. Li, L. Cai, Superhydrophobic surfaces fabricated by microstructuring of stainless steel using a femtosecond laser, Appl. Surf. Sci. 256 (2009) 61–66, https://doi.org/10.1016/j.apsusc.2009.07.061.
[16] J. Long, P. Fan, D. Gong, D. Jiang, H. Zhang, L. Li, M. Zhong, Superhydrophobic surfaces fabricated by femtosecond laser with tunable water adhesion: From lotus leaf to rose petal, ACS Appl. Mater. Interfaces 7 (2015) 9858–9865, https://doi.org/10.1021/acsami.5b01870.
[17] J. Long, L. Pan, P. Fan, D. Gong, D. Jiang, H. Zhang, L. Li, M. Zhong, Cassie-state stability of metallic superhydrophobic surfaces with various micro/nanostructures produced by a femtosecond laser, Langmuir 32 (2016) 1065–1072, https://doi.org/10.1021/acs.langmuir.5b04329.
[18] F. Chen, D. Zhang, Q. Yang, J. Yong, G. Du, J. Si, F. Yun, X. Hou, Bioinspired wetting surface via laser microfabrication, ACS Appl. Mater. Interfaces. 5 (2013) 6777–6792, https://doi.org/10.1021/am401677z.
[19] C. Guo, A.Y. Vorobyev, Ultra-short duration laser methods for the nanostructuring of materials, US20080216926 A1, 2008. doi: US 2013/0154292 A1.
[20] A.Y. Vorobyev, C. Guo, Multifunctional surfaces produced by femtosecond laser pulses, J. Appl. Phys. 117 (2015), https://doi.org/10.1063/1.4905616.
[21] B. Liu, W. Wang, G. Jiang, X. Mei, Z. Wang, K. Wang, J. Cui, Study on hierarchical structured PDMS for surface super-hydrophobicity using imprinting with ultrafast laser structured models, Appl. Surf. Sci. 364 (2016) 528–538, https://doi.org/10.1016/j.apsusc.2015.12.190.
[22] R. Jagdheesh, B. Pathiraj, E. Karatay, G.R.B.E. Römer, A.J. Huis In'T Veld, Laser-induced nanoscale superhydrophobic structures on metal surfaces, Langmuir 27 (2011) 8464–8469, https://doi.org/10.1021/la2011088.
[23] V.D. Ta, A. Dunn, T.J. Wasley, J. Li, R.W. Kay, J. Stringer, P.J. Smith, E. Esenturk, C. Connaughton, J.D. Shephard, Laser textured surface gradients, Appl. Surf. Sci. 371 (2016) 583–589, https://doi.org/10.1016/j.apsusc.2016.03.054.
[24] R. Jagdheesh, J.J. García-Ballesteros, J.L. Ocaña, One-step fabrication of near superhydrophobic aluminum surface by nanosecond laser ablation, Appl. Surf. Sci. 374 (2016) 2–11, https://doi.org/10.1016/j.apsusc.2015.06.104.
[25] D.M. Chun, C.V. Ngo, K.M. Lee, Fast fabrication of superhydrophobic metallic surface using nanosecond laser texturing and low-temperature annealing, CIRP Ann. – Manuf. Technol. 65 (2016) 519–522, https://doi.org/10.1016/j.cirp.2016.04.019.
[26] D.V. Ta, A. Dunn, T.J. Wasley, R.W. Kay, J. Stringer, P.J. Smith, C. Connaughton, J.D. Shephard, Nanosecond laser textured superhydrophobic metallic surfaces and their chemical sensing applications, Appl. Surf. Sci. 357 (2015) 248–254, https://doi.org/10.1016/j.apsusc.2015.09.027.
[27] A. Pendurthi, S. Movafaghi, W. Wang, S. Shadman, A.P. Yalin, A.K. Kota, Fabrication of nanostructured omniphobic and superomniphobic surfaces with inexpensive CO_2 laser engraver, ACS Appl. Mater. Interfaces 9 (2017) 25656–25661, https://doi.org/10.1021/acsami.7b06924.
[28] P. Gregorčič, B. Šetina-Batič, M. Hočevar, Controlling the stainless steel surface wettability by nanosecond direct laser texturing at high fluences, Appl. Phys. A Mater. Sci. Process. 123 (2017) 1–8, https://doi.org/10.1007/s00339-017-1392-5.
[29] J. Long, M. Zhong, H. Zhang, P. Fan, Superhydrophilicity to superhydrophobicity transition of picosecond laser microstructured aluminum in ambient air, J. Colloid Interface Sci. 441 (2015) 1–9, https://doi.org/10.1016/j.jcis.2014.11.015.
[30] C.V. Ngo, D.M. Chun, Effect of heat treatment temperature on the wettability transition from hydrophilic to superhydrophobic on laser-ablated metallic surfaces, Adv. Eng. Mater. 20 (2018) 1–11, https://doi.org/10.1002/adem.201701086.
[31] C.V. Ngo, D.M. Chun, Control of laser-ablated aluminum surface wettability to superhydrophobic or superhydrophilic through simple heat treatment or water boiling post-processing, Appl. Surf. Sci. 435 (2018) 974–982, https://doi.org/10.1016/j.apsusc.2017.11.185.
[32] Z. Lian, J. Xu, Z. Yu, P. Yu, H. Yu, A simple two-step approach for the fabrication of bio-inspired superhydrophobic and anisotropic wetting surfaces having corrosion resistance, J. Alloys Compd. 793 (2019) 326–335, https://doi.org/10.1016/j.jallcom.2019.04.169.
[33] A. Samanta, Q. Wang, S.K. Shaw, H. Ding, Nanostructuring of laser textured surface to achieve superhydrophobicity on engineering metal surface, J. Laser Appl. 31 (2019) 022515, https://doi.org/10.2351/1.5096148.
[34] Q. Wang, A. Samanta, F. Toor, S. Shaw, H. Ding, Colorizing Ti-6Al-4V surface via high-throughput laser surface nanostructuring, J. Manuf. Process. (2019), https://doi.org/10.1016/j.jmapro.2019.03.050.
[35] Y. Liu, Z. Zhang, H. Hu, H. Hu, A. Samanta, Q. Wang, H. Ding, An experimental study to characterize a surface treated with a novel laser surface texturing technique: Water repellency and reduced ice adhesion, Surf. Coatings Technol. 374 (2019) 634–644, https://doi.org/10.1016/j.surfcoat.2019.06.046.
[36] H. Ding, Q. Wang, A. Samanta, N. Shen, Nanosecond laser-based high-throughput surface nano-structuring (nHSN) process, US20190054571A1, 2019.
[37] M. Martínez-Calderon, A. Rodríguez, A. Dias-Ponte, M.C. Morant-Miñana, M. Gómez-Aranzadi, S.M. Olaizola, Femtosecond laser fabrication of highly hydrophobic stainless steel surface with hierarchical structures fabricated by combining ordered microstructures and LIPSS, Appl. Surf. Sci. 374 (2016) 81–89, https://doi.org/10.1016/j.apsusc.2015.09.261.
[38] M.V. Rukosuyev, J. Lee, S.J. Cho, G. Lim, M.B.G. Jun, One-step fabrication of superhydrophobic hierarchical structures by femtosecond laser ablation, Appl. Surf. Sci. 313 (2014) 411–417, https://doi.org/10.1016/j.apsusc.2014.05.224.
[39] S. Sarbada, Y.C. Shin, Superhydrophobic contoured surfaces created on metal and polymer using a femtosecond laser, Appl. Surf. Sci. 405 (2017) 465–475, https://doi.org/10.1016/j.apsusc.2017.02.019.
[40] M. Tang, V. Shim, Z.Y. Pan, Y.S. Choo, M.H. Hong, Laser ablation of metal substrates for super-hydrophobic effect, J. Laser Micro Nanoeng. 6 (2011) 6–9, https://doi.org/10.2961/jlmn.2011.01.0002.
[41] T. Chen, H.H. Liu, H. Yang, W. Yan, W. Zhu, H.H. Liu, Biomimetic fabrication of robust self-assembly superhydrophobic surfaces with corrosion resistance properties on stainless steel substrate, RSC Adv. 6 (2016) 43937–43949, https://doi.org/10.1039/C6RA06500G.
[42] K. Koch, W. Barthlott, Superhydrophobic and superhydrophilic plant surfaces: An inspiration for biomimetic materials, Philos. Trans. R. Soc. A Math. Phys. Eng. Sci. 367 (2009) 1487–1509, https://doi.org/10.1098/rsta.2009.0022.
[43] A. Steele, B.K. Nayak, A. Davis, M.C. Gupta, E. Loth, S. Adam, K.N. Barada, D. Alexander, C.G. Mool, L. Eric, Linear abrasion of a titanium superhydrophobic surface prepared by ultrafast laser microtexturing, J. Micromech. Microeng. 23 (2013) 115012, https://doi.org/10.1088/0960-1317/23/11/115012.
[44] M.K. Tang, X.J. Huang, Z. Guo, J.G. Yu, X.W. Li, Q.X. Zhang, Fabrication of robust and stable superhydrophobic surface by a convenient, low-cost and efficient laser marking approach, Colloids Surf. A Physicochem. Eng. Asp. 484 (2015) 449–456, https://doi.org/10.1016/j.colsurfa.2015.08.029.
[45] F.M. Chang, S.L. Cheng, S.J. Hong, Y.J. Sheng, H.K. Tsao, Superhydrophilicity to superhydrophobicity transition of CuO nanowire films, Appl. Phys. Lett. 96 (2010) 2008–2011, https://doi.org/10.1063/1.3360847.

[46] J.E. O'Gara, B.A. Alden, C.A. Gendreau, P.C. Iraneta, T.H. Walter, Dependence of cyano bonded phase hydrolytic stability on ligand structure and solution pH, J. Chromatogr. A. 893 (2000) 245–251, https://doi.org/10.1016/S0021-9673(00)00696-8.

[47] M.H. Nada, S.C. Larsen, Insight into seed-assisted template free synthesis of ZSM-5 zeolites, Microporous Mesoporous Mater. 239 (2017) 444–452, https://doi.org/10.1016/j.micromeso.2016.10.040.

[48] Z. Chu, S. Seeger, Superamphiphobic surfaces, Chem. Soc. Rev. 43 (2014) 2784–2798, https://doi.org/10.1039/C3CS60415B.

[49] A. Cunha, A.P. Serro, V. Oliveira, A. Almeida, R. Vilar, M.C. Durrieu, Wetting behaviour of femtosecond laser textured Ti-6Al-4V surfaces, Appl. Surf. Sci. 265 (2013) 688–696, https://doi.org/10.1016/j.apsusc.2012.11.085.